WCTE 2020
WORLD CONFERENCE ON TIMBER ENGINEERING
SANTIAGO, CHILE | 24 - 27 AUGUST

HEAT AND MASS TRANSFER MODEL FOR WOOD INCLUDING FREE WATER TRANSPORT

Maximilian Autengruber[1], Markus Lukacevic[1], Josef Füssl[1]

ABSTRACT: Knowledge about wood moisture conditions in a timber component is essential to predict its mechanical behavior. Not only stiffness and strength properties are highly dependent on wood moisture content but also diffusion coefficients, density, specific heat capacity and the thermal conductivity. Therefore, modern prediction tools, which are able to describe these effects, can benefit the development of new wood-based products. Especially, if they exhibit complex geometries and are made of materials with different moisture characteristics, as different and direction-dependent coefficients of expansion may lead to critical stresses.

Transport mechanisms below the fiber saturation point were developed by [1-2]. Three coupled differential equations describe bound water, water vapor and energy conservation. Free water exists above the fiber saturation point with the corresponding transport mechanisms described in [3]. Values of the free water content can be much higher than those of bound water and water vapor. Thus, within the areas, where the switch from the transport mechanisms below the fiber saturation point to those above occur, high gradients can exist. To deal with these within the finite element method different procedures, like upstreaming and mass lumping [4], were used. A three-dimensional Abaqus User-Element Subroutine was developed to describe these coupled equations.

KEYWORDS: moisture transfer model, free water, drying, wetting, moisture induced failure

1 INTRODUCTION

Wood is a naturally grown building material with highly moisture-dependent material properties, which in addition also vary in the material directions. Increases in moisture content (MC) within wood on one hand lead to decreasing stiffness and strength properties and on the other hand lead to dimensional changes caused by swelling. Due to the non-uniform expansion of wood in its orthotropic material directions, which compared to other building materials can be quite substantial, the resulting stresses can cause cracks. In general, water can be present in three different states in wood: bound water in the cell walls, water vapor and free water in the lumens. These states are interacting with each other.

Although dimensional changes of wood are linked to changes in bound water concentration only and free water only exists above the so-called fiber saturation point, such a full description of water states within wood might be necessary. For example, if wood is used as a scaffold material for concrete constructions, timber beams and plates are subjected to not only outdoor weathering but are also often stored unsheltered, where they might end up lying in puddles for a long time. Another possible use case of such a model is the simulation of the direct application of fresh concrete to notched CLT slabs for the construction of timber-concrete composite structures.

The transport processes below the so-called fiber saturation point (FSP) can be well described [1-2,5-7] by a multi-Fickian transport, i.e. by separating bound water and water vapor transport mechanisms and by coupling them via the so-called sorption. It has been shown that such an implementation is essential when moisture distributions in wood specimens thicker than a few millimeters or subjected to higher relative humidity levels are to be predicted correctly. In contrast to other porous media, in wood the bound water phase cannot be easily coupled to the free water phase, as wood is highly hygroscopic [3] and the amounts of water in the two phases differs greatly [10].

We combined the mathematical model for free water transport above the FSP with the multi-Fickian approaches below the FSP [11], where the numerically challenging transition of the transport mechanisms needs special attention in the implementation [12-14].

The developed model can then easily be combined with other developments of our research group in the field of computational wood mechanics [15-16]. For example, the moisture uptake and distribution in various wood (products) cross sections and their susceptibility to cracking can be studied with wood-specific failure criteria [17-20].

Within this paper, first, the heat and mass transfer model for wood is presented in Section 2. In Section 3, a

[1] Maximilian Autengruber, Vienna University of Technology (TU Wien), Austria, maximilian.autengruber@tuwien.ac.at
Markus Lukacevic, Vienna University of Technology (TU Wien), Austria, markus.lukacevic@tuwien.ac.at
Josef Füssl, Vienna University of Technology (TU Wien), Austria, josef.fuessl@tuwien.ac.at

validation example shows the model's capability to reproduce the correct transition of transport processes from above to below the FSP. Next, in Section 4, two applications to civil engineering problems are presented, where the first one shows how historic climate data can be used to study the moisture distribution and subsequent susceptibility to cracking in wood cross sections. The second application is the simulation of the critical moisture uptake in notched timber-concrete composite floors, when fresh concrete gets in contact with end-grain surfaces. Finally, in the last section the paper is concluded and an outlook to future research is given.

2 HEAT AND MASS TRANSFER MODEL FOR WOOD

Wood has a cellular structure, where the so-called lumens are enclosed by the hygroscopic cell walls, which are oriented in longitudinal direction and connected at their ends by pits. For green wood, these pits are open and allow an unrestricted flow of free water, but during the technical drying of wood, they get mostly closed. Such aspirated pits can deaspirate, if they get in contact with water again, but in experiments information on the amount of closed or open pits is often not available, which adds an additional layer of difficulty in the validation process.

When the relative humidity in the environment of a wood sample increases, moisture enters through pores into the wood, where the moisture is both transported through the lumens and adsorbed by the cell walls, where it is also transported in terms of bound water. Thus, in general water can be present in wood in three different states: water vapor as well as bound and free water. These interact with each other, as they all tend to reach an equilibrium state.

As already mentioned, the transport mechanisms below the FSP of coupled water vapor and bound water transport are modeled using a multi-Fickian approach. For the transport of the free water above the FSP, our model uses Darcy's law, where the driving force is the gradient of capillary pressure.

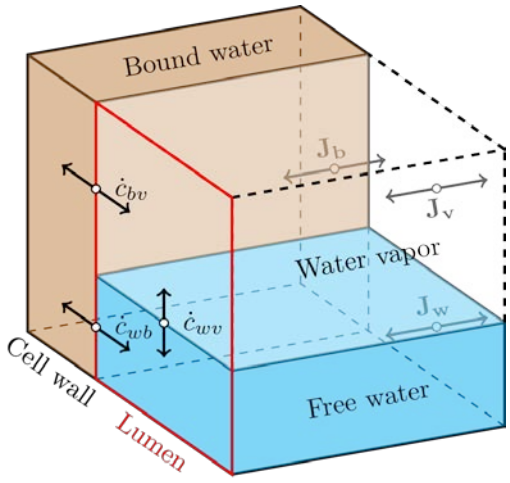

Figure 1: *Volume-averaged interactions between the three phases of water: bound water, water vapor and free water; and definition of fluxes of the same components via the boundaries of the RVE [11]*

As in [21], a representative volume element (RVE) is defined for the description of the different transfer mechanisms (see Figure 1): bound water c_b exists in the cell wall, water vapor c_v and free water c_w in the lumen. The coupling mechanisms between the phases are sorption $\dot{c}_{wb}$ from free water to bound water and sorption $\dot{c}_{bv}$ from water vapor to bound water, as well as evaporation/condensation $\dot{c}_{wv}$ between free water and water vapor. The fluxes via the boundaries of the RVE are free water flux $\boldsymbol{J}_w$, bound water flux $\boldsymbol{J}_b$ and water vapor flux $\boldsymbol{J}_v$. In addition to the mass conservation equations, a total energy conservation equation with the process of thermal conduction with the heat flux $\boldsymbol{f}$ is also included. The governing equations are:

Conservation of bound water concentration:

$$\frac{\partial c_b}{\partial t} = -\frac{\partial}{\partial x}\boldsymbol{J}_b + \dot{c}_{bv} + \dot{c}_{wb} \tag{1}$$

Conservation of water vapor concentration:

$$\frac{\partial c_v}{\partial t} = -\frac{\partial}{\partial x}\boldsymbol{J}_v - \dot{c}_{bv} + \dot{c}_{wv} \tag{2}$$

Conservation of free water concentration:

$$\frac{\partial c_w}{\partial t} = -\frac{\partial}{\partial x}\boldsymbol{J}_w - \dot{c}_{wb} - \dot{c}_{wv} \tag{3}$$

Conservation of energy:

$$\begin{aligned}\frac{\partial \rho \cdot h}{\partial t} = &+\frac{\partial}{\partial x}\boldsymbol{f} - \frac{\partial}{\partial x}\boldsymbol{J}_b\bar{h}_b - \frac{\partial}{\partial x}\boldsymbol{J}_v h_v - \frac{\partial}{\partial x}\boldsymbol{J}_w h_w \\ &+ \dot{c}_{bv}(h_v - h_b) + \dot{c}_{wb}(h_w - h_b) \\ &+ \dot{c}_{wv}(h_w - h_v)\end{aligned} \tag{4}$$

where the left-hand terms account for changes of concentration and energy over time, respectively. $\bar{h}_b$ is the averaged enthalpy of bound water and h_b the specific enthalpy of bound water. h_v and h_w are the specific enthalpies of water vapor and water, respectively.

All previously described transport mechanisms, except for the bound water one, are affected by the surrounding climate. This means that exchange of masses and heat across the boundaries of the sample can take place in terms of heat, free water and water vapor. When wood gets in contact with free water, its flux ϕ_w across the boundary can be determined as

$$\phi_w = k_{cw}(c_w - c_{w,0})\, f_{lum}, \tag{5}$$

where k_{cw} considers a possible resistance due to coatings and $c_{w,0}$ the water concentration of the surroundings.

In case of drying and wetting with no free water present, only a boundary condition for water vapor is taken into account:

$$\phi_v = k_{cv}(c_v - c_{v,0})\, f_{lum}, \tag{6}$$

where k_{cv} is a film boundary coefficient, which considers airflow and convection with respect to air speed and surface roughness, and $c_{v,o}$ is the water vapor concentration in distant air. For more details of the full implementation, refer to [11].

The large differences in the amounts of water in areas, where the transition from transport mechanisms below the fiber saturation point to those above occur, lead to several

numerical challenges, which had to be tackled by applying the following methods: upstream weighting, mass lumping and the use of a mixed formulation for the free water flow, i.e. a combination of a concentration-based and a pressure-based formulation.
The stable and reliable simulation algorithm is fully implemented in a three-dimensional Abaqus (from Dassault Systèmes, Vélizy-Villacoublay, France) User Element Subroutine.

3 MODEL VALIDATION

Important parts of the presented approach, i.e. the multi-Fickian model below the FSP, are broadly used and have been validated in several works [1-2,5-7]. Thus, here the focus is on showing that conditions above the FSP and the transition from above to below the FSP can be modeled realistically.
Thus, we simulate a one-dimensional drying process in radial direction starting from 100 % MC, which has been used in [22] with different numerical and analytical models. Therefore, two reference solutions are available and plotted in Figure 2: a model with constant diffusivity (black curves) and one with variable diffusivity (blue curves). For both only two degrees of freedom were used by combining all moisture-related ones into a single DOF. As shown in the figure, the specimen length was 20 mm. The initial MC in the sample is 100 % and the initial temperature 298.15 K. The film boundary coefficient for heat transfer k_T is 14 W/m^{2}K and the one for mass transfer k_{cv} is 0.014 m/s, respectively. The parameters for the sorption isotherm were fitted to the equation in [3] at a temperature of 323.15 K, resulting in the following values for the Hailwood-Horrobin model: $f_1 = 2.038$, $f_2 = 11.08$ and $f_3 = -9.689$. The dry density of the wood sample was 500 kg/m^3. To model the capillary pressure, the expression from [3] was used:

$$P_c = 1.364 \cdot 10^5 \, \sigma \, (c_w + 1.2 \cdot 10^{-4})^{-0.61}, \qquad (7)$$

where σ is the surface tension of water.
The surrounding climate is now set to a temperature of 323.15 K and 32 % relative humidity, which corresponds to an equilibrium MC of approximately 7 %, and the resulting heat and moisture transport in the wood sample is simulated.
The FE model consisted of 40 elements with characteristic dimensions from 0.2 mm (close to the boundary surface) to 1 mm. This resulted in a total of 164 nodes. A total CPU time of 210 s was needed to simulate the 50 h of drying, with 797 increments and maximum time step sizes of 360 s.
The comparison of the presented model to the models in [22] in Figure 2 shows that the simulation results are very similar for the first 15 hours. The plateau in the temperature curves corresponds to the effect of the so-called wet-bulb temperature, i.e. the temperature is constant as long as free water exists, because the entire energy is needed to evaporate the free water. Thus, as soon as the MC at reference point ①, i.e. at the boundary surface, drops below the FSP, the temperature starts to increase to the dry bulb temperature.

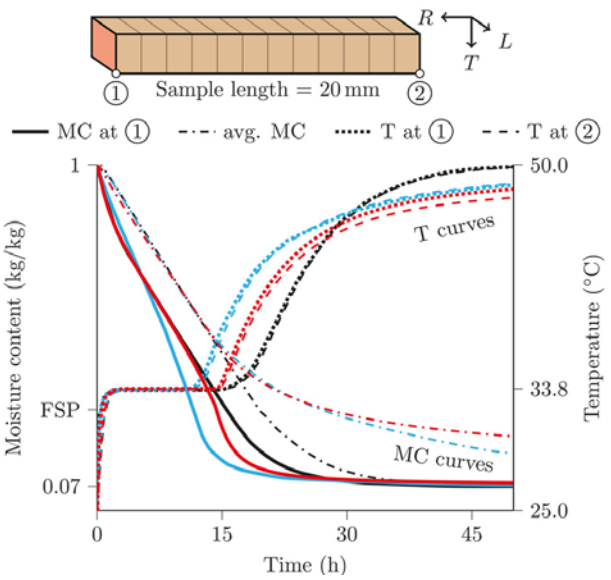

Figure 2: *Time history of moisture content (MC) and temperature (T) during 50h of 1D drying in radial direction. Comparison of the presented model (red) and of the models from [22] with constant (black) and variable (blue) diffusivity [11]*

For the simulation period after the first 15 hours, differences between the models can be noticed. These can be explained by the different treatment of the three phases of water and their diffusion parameters (variable or constant). For the temperature curves, the differences in the models are smaller, as the high thermal conductivity has less effect on the simulations than the moisture transport properties.
In [11] several additional validation examples show the overall very good performance by means of comparisons to both drying and infiltration simulations and experiments. Furthermore, a mesh study and parameter studies confirmed the robustness and good convergence characterisitics of the presented heat and moisture transport model for wood.

4 APPLICATION TO CIVIL ENGINEERING PROBLEMS

In the following, the application of our heat and moisture transport simulation tool to two civil engineering problems is shown. In the first one, we use our model together with easily available historic climate data to simulate realistic moisture distributions in various cross sections over a longer time period. In the second one, we show that the realistic consideration of free water transport mechanisms in wood is important, when you study the detailed effects of fresh concrete application on the moisture distribution in timber-concrete composite (TCC) floors with notched connections.

4.1 Time history of moisture profiles for different cross sections

In the first example, the moisture uptake and distribution within various wood (product) cross sections and their susceptibility to cracking was studied (see Figure 3).

Here, moisture profiles of two cross sections subjected to realistic outdoor climate conditions over the time span of a full year are shown. Thus, critical time points can be identified and studied in more detail.
Such realistic moisture calculations allow in a next step to also conduct stress calculations. In combination with a multi-surface failure criterion for wood [17-18], it is then possible to evaluate the exposure of wooden structures to realistic climate conditions.

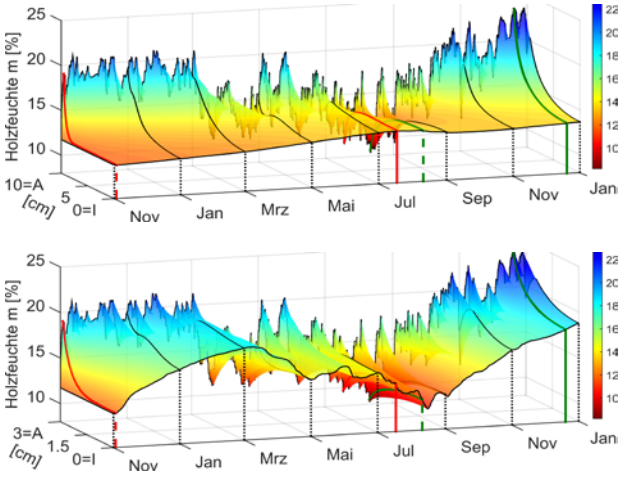

Figure 3: *Moisture (Holzfeuchte) profiles for two different cross sections, where the point A is a point on the outer surface and the point I the center point. The top profile belongs to a GLT beam with dimensions of 20x40cm and the bottom one to a timber beam with 6x8cm.*

Figure 4 shows such a possible approach, which was used in [23] to employ realistic climate data in the investigation of the moisture-induced cracking behavior of cross sections. Thus, the difference in various timber dimensions and, in future, also in location-specific behavior can be studied in detail. Based on the moisture fields (see Figure 4a), the cross sections' expansion due to swelling and shrinkage was determined with linear elastic simulations. In each integration point and for all simulation increments the abovementioned multi-surface failure criterion was evaluated (see Figure 4b). For each integration point violating this criterion, the corresponding volume was added up, resulting in *crack-prone volumes* per time point. This results in a graph of this volume over the simulation time (Figure 4c). At two distinct peaks of this graph, one for the summer period (MC at the boundary is higher than at the center) and one for the winter period (MC at the boundary is lower than at the center), simulations with the extended finite element method (XFEM) were performed (see Figure 4d) to find the most critical moisture-induced stress situations, which would result in cracks.
It was shown that the relationship between the resulting crack-free widths and the total cross section widths were quite linear for the summer periods. This means they are in good agreement with the definition of k_{cr} in Eurocode 5, which defines how to consider possible cracks by reducing the cross section width in shear resistance calculations. However, the standard under-estimates the numerically predicted widths by about 10 %. For the wetting case, i.e. for cracks in the interior of cross sections, which is not covered by Eurocode 5, also a linear relationship was found.

4.2 Effect of fresh concrete application on moisture distribution in notched TCC floors

Another civil engineering application of our model is the investigation of the effect of applying fresh concrete on cross-laminated timber (CLT) plates with notches (see Figure 5). Such notches in timber-concrete composite floors are used increasingly as shear connectors, as other types of connectors are either expensive or labor-intensive in their application. These notches are created by milling grooves into the uppermost lamella of the timber slabs. When cast-in-place concrete is now poured onto the CLT plate, the newly created end-grain surfaces are especially prone to moisture penetration. To avoid the possibility of moisture-induced failure within the CLT plates, caused by the bleeding of the fresh concrete, oftentimes a separating foil is placed on top of the timber component. As this usually involves a considerable amount of manual labor and might also decrease the efficiency of the notched shear connection by reducing friction properties, we now study the actual amount of moisture uptake in such a scenario and its cumulative effects during the first two years after installation, when subjected to an additional indoor climate.

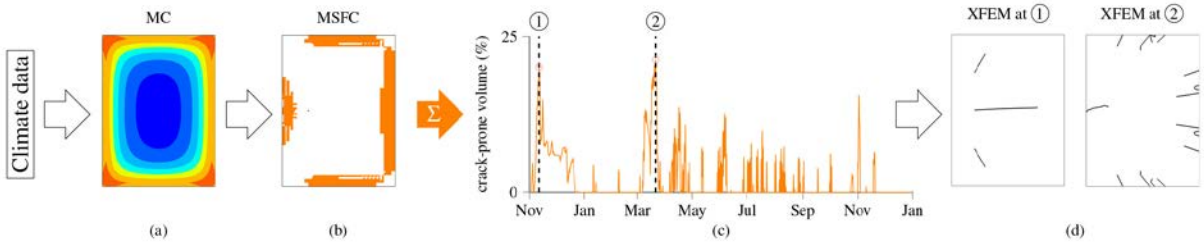

Figure 4: *Schematic description for the identification of crack-prone regions and critical points in time. Based on climate data, for various cross sections (a) moisture fields and resulting stress states were simulated. Next, (b) a multisurface failure criterion was evaluated in each integration point to identify crack-prone regions. (c) The corresponding crack-prone volumes were then added up and plotted versus the time domain. At two specific peaks, 1 for the winter and 2 for the summer period, (d) XFEM simulations were performed to determine crack patterns. [23]*

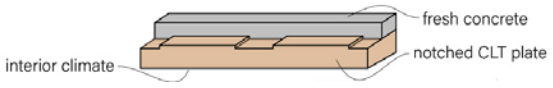

Figure 5: *Application of cast-in-place concrete on a notched CLT plate, resulting in moisture loads for the latter. In addition, after installation the floor's bottom surface is subjected to a two-year indoor climate to simulate moisture accumulations and the impeded moisture reduction*

We use the experimental results from [24] to obtain realistic moisture loads from the bleeding of the fresh concrete and its interaction with the free wood surfaces. In fact, the courses of the mass transfer coefficients for water vapor k_{cv} and free water k_{cw}, respectively, which were introduced in Equations (5) and (6), are calibrated. In [24] the moisture contents in the upper three lamellas were measured for 15 TCC specimens (various configurations and concrete mixtures) and over a period of 28 days after the application of the fresh concrete. The specimens represented a section of a TCC floor system and had either a flat surface on the upper side or a 1.5 cm notch in the uppermost lamella, leading to a vertical notch surface, i.e. an end-grain surface. To measure the moisture transport in the wood, two moisture sensors were installed in the middle of each of the upper three lamellas.

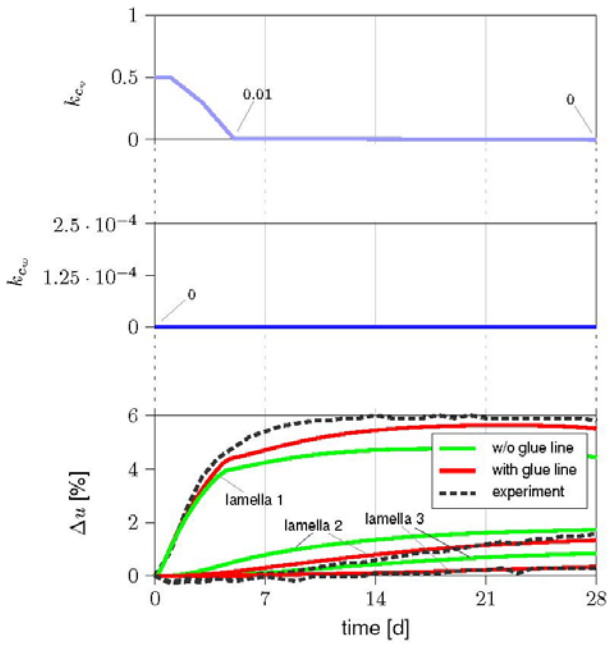

Figure 6: *Horizontal timber/concrete surfaces: Calibrated course of the mass transfer coefficients for water vapor k_{cv} and free water k_{cw} in [m/s], respectively, and development of the resulting changes in moisture content Δu in [%] in comparison to experimental values [25]*

As the moisture transport in wood is much greater in longitudinal direction than the transversal ones, we first use the measurements for the specimens with flat top CLT surfaces to calibrate the coefficients in vertical, i.e. radial, direction. Figure 6 shows the resulting course of the two mass transfer coefficients, i.e. no free water transport is present in this case. This leads to the changes in moisture content in the three monitored locations shown in the lower plot of the same figure. Here also the difference in considering (red curves) and neglecting (green curves) the reduced permeability caused by the glue lines can be noticed. Omitting the adhesive would lead to too low moisture levels in the uppermost lamella and overestimate the moisture input into the following two lamellas, respectively.

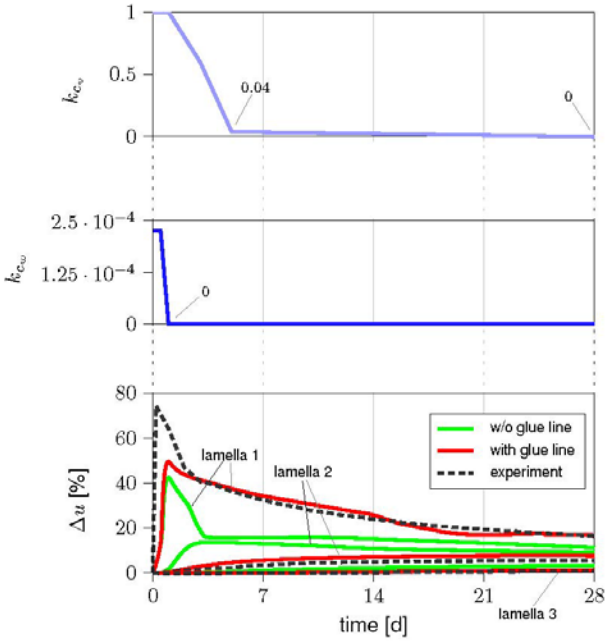

Figure 7: *Vertical timber/concrete surfaces (=end-grain surfaces): calibrated course of the mass transfer coefficients for water vapor k_{cv} and free water k_{cw} in [m/s], respectively, and development of the resulting changes in moisture content Δu in [%] in comparison to experimental values [25]*

In the next step, the mass transfer coefficients in longitudinal direction, which are applied to the end-grain surfaces, are calibrated using another experimental result from [24]. The mass transfer coefficients for free water k_{cw} is now nonzero for the first two days. This enables the realistic modeling of the moisture input from the concrete in the area of the notch, which leads to moisture contents exceeding the FSP. Again, omission of the glue line permeability would lead to a too fast moisture transport into the lower lamellas.

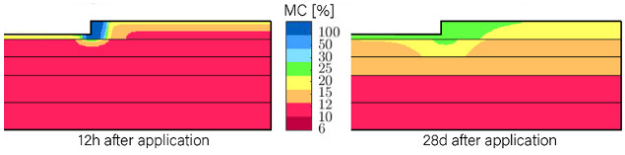

Figure 8: *Moisture distribution in CLT plate after 12 hours and 28 days of application of fresh concrete*

After application of the cast-in-place concrete, the moisture distribution in the CLT plate is simulated for the

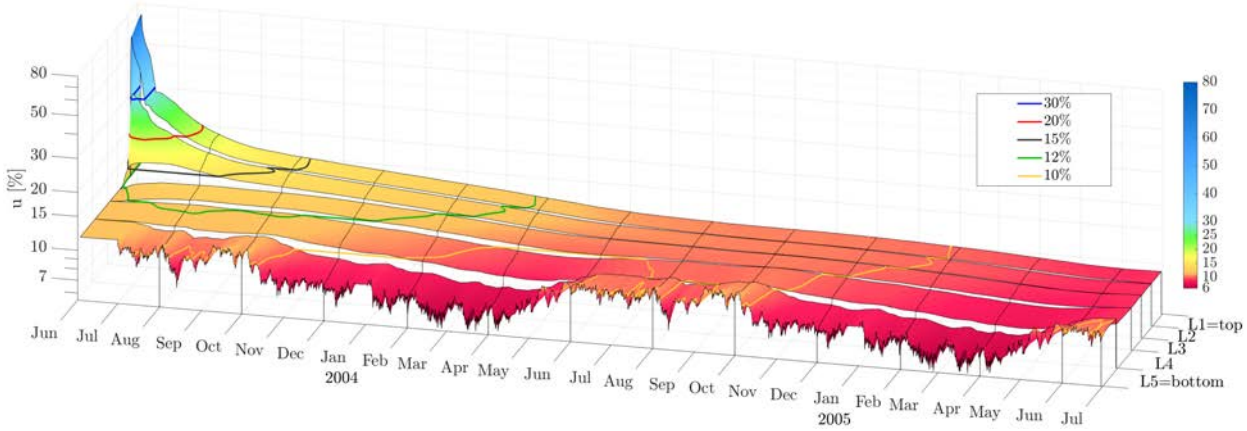

Figure 9: *Wood moisture distribution over the thickness of the CLT plate (divided into the five lamellas) after application of fresh concrete on the notched top surface and of a wet two-year indoor climate on the bottom surface after the first 28 days, shown for a total simulation period of 25 months [25]*

first 28 days. The resulting moisture states after 12 hours and 28 days, respectively, are shown in Figure 8. It can be clearly noticed that the initial moisture uptake is dominating in the region of the end-grain surfaces, where moisture contents exceeding the FSP arise. In addition, the retention behavior of the glue line, resulting in the accumulation of moisture in the uppermost lamella, can be observed.

After the first 28 days, which corresponds to the curing time of the concrete, we assume that the TCC floor is installed at the construction site and apply an additional moisture load, representing a realistic 2-year indoor climate, to the bottom surface of the CLT plate. The used climate is the time course of relative humidity and temperature of a kitchen in a student dormitory. This application of a rather wet climate leads to the course of the moisture distribution over the CLT plate height shown in Figure 9. After installation of the floor system at the construction site (28 d after start of simulation = July 1st, 2003), the moisture content in the uppermost lamella (L1 in Figure 9) and parts of the second lamella (L2) still exceeds 20 %. At the bottom of the third lamella (L3) the moisture content is already at 12 %, which corresponds to the equilibrium moisture content at the start of the simulation. The increased moisture content in L1 decreases quickly after installation and is below the marked (red contour line) MC of 20 % after approximately three weeks. After that, the moisture content in L1 slowly decreases further. The influence of the applied indoor climate can be observed for the first time when the 12 % level is reached. In general, the application of fresh concrete mostly influences the two uppermost lamellas for about the first nine months after installation. This might lead to problematic situations as the region with increased moisture contents coincides with the region with the highest shear stresses. Loads are transferred via the notched shear connection to the CLT plate in a region, where increased moisture contents might reduce the shear strength.

To study a possible low-cost solution of this problem, in [25] we further investigate the influence of a local sealing of the end-grain surfaces or compare the moisture distributions to the case of using precast concrete slabs, where no bleeding of the concrete takes place.

5 CONCLUSION AND OUTLOOK

We presented a unified moisture transport model for wood, which is able to capture mechanisms both below and above the FSP realistically. By including the free water contribution in the moisture simulations, not only the water uptake but also the possible accumulation of free water in wooden parts, which are in direct contact to water, can be considered. Those might lead to delayed drying in critical regions and, therefore, must be considered in such simulations. The implementation of all mechanisms is numerically challenging as high gradients and sudden changes in MC can occur. To overcome these difficulties, several techniques were implemented, leading to a stable and reliable simulation tool, which has been programmed as a user element subroutine in the commercial FE software Abaqus.

The presented application examples of our simulation tool to civil engineering problems shows the breadth of possible future use cases. By applying the resulting moisture fields as loads in timber engineering simulations, we can resort to several other developments of ours in the field of computational mechanics, such as the simulation of fracture mechanisms [17-20,23] or stochastic phenomena in timber engineering [26-28].

Thus, the probability of failure due to moisture can be assessed already during the development and planning phase and, therefore, reasonable design changes can be initiated in time.

ACKNOWLEDGEMENT

This work was supported by the FWF Austrian Science Fund through the START grant Y1093 and the ERA-NET Cofund Action ‘ForestValue’.

REFERENCES

[1] K. Krabbenhøft, L. Damkilde: A model for non-fickian moisture transfer in wood, *Materials and Structures*, 37(9):615–622, 2004.

[2] E. S. Fortino, A. Genoese, A. Genoese, L. Nunes, P. Palma: Numerical modelling of the hygro-thermal response of timber bridges during their service life: A monitoring case-study, *Construction and Building Materials*, 47:1225–1234, 2013.

[3] P. Perré, I.W. Turner: A 3-d version of TransPore: a comprehensive heat and mass transfer computational model for simulating the drying of porous media, *Int J Heat Mass Transfer*, 42:4501–21, 1999.

[4] J. Eriksson: Study of Moisture Flow and Moisture-Induced Distortions in Sawn Boards and Laminated Timber Products., PhD thesis, Chalmers University of Technology, Gothenburg, 2004.

[5] D. Konopka, M. Kaliske: Transient multi-Fickian hygro-mechanical analysis of wood, *Comput. Struct.* 197:12–27, 2018.

[6] H.L. Frandsen, L. Damkilde, S. Svensson: A revised multi-Fickian moisture transport model to describe non-Fickian effects in wood, *Holzforschung* 61:563–572, 2007.

[7] J. Eitelberger, K. Hofstetter, S. Dvinskikh: A multi-scale approach for simulation of transient moisture transport processes in wood below the fiber saturation point, *Compos. Sci. Technol.* 71(15):1727–1738, 2011.

[8] C. Gebhardt, D. Konopka, A. Börner, M. Mäder, M. Kaliske: Hygro-mechanical numerical investigations of a wooden panel painting from Katharinenaltar by Lucas Cranach the elder, *J. Cult. Heritage* 29:1–9, 2018.

[9] S. Fortino, P. Hradil, A. Genoese, A. Genoese, A. Pousette: Numerical hygro-thermal analysis of coated wooden bridge members exposed to northern European climates, *Constr. Build. Mater.* 208:492–505, 2019.

[10] D. Gawin, C.E. Majorana, B.A. Schrefler: Numerical analysis of hygro-thermal behaviour and damage of concrete at high temperature, *Mech. Cohes –Frict. Mater.* 4(1):37–74, 1999.

[11] M. Autengruber, M. Lukacevic, J. Füssl,: Finite-element-based moisture transport model for wood including free water above the fiber saturation point, *International Journal of Heat and Mass Transfer* 161:120228, 2020

[12] K. Krabbenhøft: Moisture Transport in Wood –A Study of physical-Mathematical Models and Their Numerical Implementation, Ph.D thesis, Technical University of Denmark, 2003.

[13] P.A. Forsyth, M.C. Kropinski: Monotonicity considerations for saturated–unsaturated subsurface flow, SIAM J. Sci. Comput. 18(5):1328–1354, 1997.

[14] M.A. Celia, E.T. Bouloutas, R.L. Zarba: A general mass-conservative numerical solution for the unsaturated flow equation, *Water Resour. Res.* 26(7):1483–1496, 1990.

[15] M. Lukacevic, J. Füssl: Numerical simulation tool for wooden boards with a physically based approach to identify structural failure, *Eur. J. Wood Wood Prod.* 72(4):497–508, 2014.

[16] M. Lukacevic, G. Kandler, M. Hu, A. Olsson, J. Füssl: A 3D model for knots and related fiber deviations in sawn timber for prediction of mechanical properties of boards, *Mater. Des.* 166:107617, 2019.

[17] M. Lukacevic, J. Füssl, R. Lampert: Failure mechanisms of clear wood identified at wood cell level by an approach based on the extended finite element method, *Eng. Fract. Mech.* 144:158–175, 2015.

[18] M. Lukacevic, W. Lederer, J. Füssl: A microstructure-based multisurface failure criterion for the description of brittle and ductile failure mechanisms of clear-wood, *Eng. Fract. Mech.* 176:83–99, 2017.

[19] J. Füssl, M. Li, M. Lukacevic, J. Eberhardsteiner, C.M. Martin: Comparison of unit cell-based computational methods for predicting the strength of wood, *Eng. Struct.* 141:427–443, 2017.

[20] M. Li, J. Füssl, M. Lukacevic, J. Eberhardsteiner, C.M. Martin: Strength predictions of clear wood at multiple scales using numerical limit analysis approaches, *Comput. Struct.* 196:200–216, 2018.

[21] S. Whitaker, J.P. Hartnett, T.F. Irvine: Simultaneous heat, mass, and momentum transfer in porous media: A theory of drying, *Advances in Heat Transfer* 13:119–203, 1977.

[22] P. Perré: The proper use of mass diffusion equations in drying modeling: Introducing the drying intensity number, *Dry Technol* 33(15–16):1949–1962, 2015.

[23] M. Autengruber, M. Lukacevic, C. Gröstlinger, J. Füssl: Finite-element-based prediction of moisture-induced crack patterns for 18 cross sections of solid wood and glued laminated timber exposed to a realistic climate condition, *Construction and Building Materials*, 2020 (under review).

[24] G. Muller: Feuchteinteraktionsverhalten von Brettsperrholz und Beton im Verbund. Master's thesis, TU Munich, 2016 (in German).

[25] M. Lukacevic, M. Autengruber, T. Raimer, J. Füssl: Effect of fresh concrete application on moisture distribution in timber-concrete composite floors with notched connections, investigated by means of numerical simulation, 2020 (in preparation).

[26] G. Kandler, M. Lukacevic, C. Zechmeister, S. Wolff, J. Füssl: Stochastic engineering framework for timber structural elements and its application to glued laminated timber beams. *Construction and Building Materials* 190:573–592, 2018.

[27] S. Pech, G. Kandler, M. Lukacevic, J. Füssl: Metamodel assisted optimization of glued laminated timber beams by using metaheuristic algorithms. *Engineering Applications of Artificial Intelligence* 79:129-141, 2019.

[28] M. Li, J. Füssl, M. Lukacevic, C.M. Martin, J. Eberhardsteiner: Bending strength predictions of cross-laminated timber plates subjected to concentrated loading using 3D finite-element-based limit analysis approaches, *Composite Structures* 220:912-925, 2019